



Myeloid-derived suppressor cells are implicated in regulating permissiveness for tumor metastasis during mouse gestation

Laetitia A. Mauti,¹ Marie-Aude Le Bitoux,¹ Karine Baumer,¹ Jean-Christophe Stehle,¹ Dela Golshayan,² Paolo Provero,³ and Ivan Stamenkovic¹

¹Division of Experimental Pathology, Institute of Pathology, Centre Hospitalier Universitaire Vaudois (CHUV), University of Lausanne, Lausanne, Switzerland.

²Transplantation Immunopathology Laboratory, Department of Medicine, University of Lausanne, Lausanne, Switzerland.

³Department of Biochemistry and Molecular Biology, University of Torino, Torino, Italy.

Metastasis depends on the ability of tumor cells to establish a relationship with the newly seeded tissue that is conducive to their survival and proliferation. However, the factors that render tissues permissive for metastatic tumor growth have yet to be fully elucidated. Breast tumors arising during pregnancy display early metastatic proclivity, raising the possibility that pregnancy may constitute a physiological condition of permissiveness for tumor dissemination. Here we have shown that during murine gestation, metastasis is enhanced regardless of tumor type, and that decreased NK cell activity is responsible for the observed increase in experimental metastasis. Gene expression changes in pregnant mouse lung and liver were shown to be similar to those detected in premetastatic sites and indicative of myeloid cell infiltration. Indeed, myeloid-derived suppressor cells (MDSCs) accumulated in pregnant mice and exerted an inhibitory effect on NK cell activity, providing a candidate mechanism for the enhanced metastatic tumor growth observed in gestant mice. Although the functions of MDSCs are not yet understood in the context of pregnancy, our observations suggest that they may represent a shared mechanism of immune suppression occurring during gestation and tumor growth.

Introduction

Metastasis is a multistage process that constitutes the primary cause of cancer-related death. It requires cells to detach from the primary tumor mass, migrate toward and invade lymphatic or blood vessels, survive within the circulation, attach to the endothelium of distant organs, penetrate the endothelial barrier, and establish new tumor colonies (1). The process is highly inefficient, as less than 0.1% of tumor cells that penetrate the circulation end up forming metastatic colonies (2, 3), but the explanation for the observed inefficiency of metastasis is still largely obscure. Several possible reasons have been invoked, including tumor cell destruction by shear stress and immune cells in the circulation (4), and it is clear that large numbers of tumor cells can penetrate distant organs only to undergo apoptosis or enter a state of dormancy that may extend for an indefinite period of time (5). Mechanisms underlying dormancy are unclear, although recent observations suggest that the new microenvironment may prevent tumor cells from proliferating while allowing them to survive, or, alternatively, that immune surveillance may keep micrometastases in check (6). Over time, modifications in the host microenvironment — including the recruitment and function of cells of the immune system — that occur as a result of a variety of physiological events, including aging, may relieve the pressure on the metastatic foci, allowing them to expand and ultimately form clinically relevant macrometastases (7).

Recent evidence suggests that tumor cells may be able to direct the formation of premetastatic niches in selected organs by secreting or by inducing stromal cell secretion of cytokines or

growth factors — collectively described as tumor-derived soluble factors (TDSFs) — that render selected target organ microenvironments permissive for the implantation and subsequent outgrowth of disseminating tumor cells (8, 9). A major constituent of premetastatic niches are bone marrow-derived cells (BMDCs), which promote local tumor cell establishment by secreting chemoattractants (10, 11), producing proteases that facilitate tumor cell infiltration of the target organ and elaborating extracellular matrix components that further help recruit BMDCs or tumor cells to these sites (9, 12). Enhanced lung metastasis may also result from experimental allergen-induced lung leukocyte infiltration and asthma has been shown to be prevalent in breast cancer patients with lung metastases (13).

Tumors also need to escape immune surveillance to grow at primary as well as at metastatic sites (14). One of the possible results of immunoediting, a process that shapes tumor cell immune resistance by selective pressure of the immune system itself, is the accumulation of cells of the myelomonocytic lineage that harbor immunosuppressive functions and repress antitumor immunity. This heterogeneous cell population of myeloid-derived suppressor cells (MDSCs) expands not only in the context of cancer (driven by TDSFs), but also during situations such as infection, autoimmune disease, vaccination, and trauma (15, 16).

Pregnancy is a physiological state of dampened cellular immunity in the context of maternal immune tolerance toward the semiallogenic conceptus (17). Several mechanisms are involved in preventing rejection of fetal tissues, including, among others, lack of classical class I MHC molecules on the surface of fetal cells, expression of NK cell- and T cell-modulating HLA-G molecules, hyporesponsiveness of immune cells as a result of indoleamine 2,3-dioxygenase activity and specific silencing of alloreactive T cells by regulatory T cells (18). MDSC activity, however, has

Authorship note: Laetitia A. Mauti and Marie-Aude Le Bitoux contributed equally to this work.

Conflict of interest: The authors have declared that no conflict of interest exists.

Citation for this article: *J Clin Invest.* 2011;121(7):2794–2807. doi:10.1172/JCI41936.

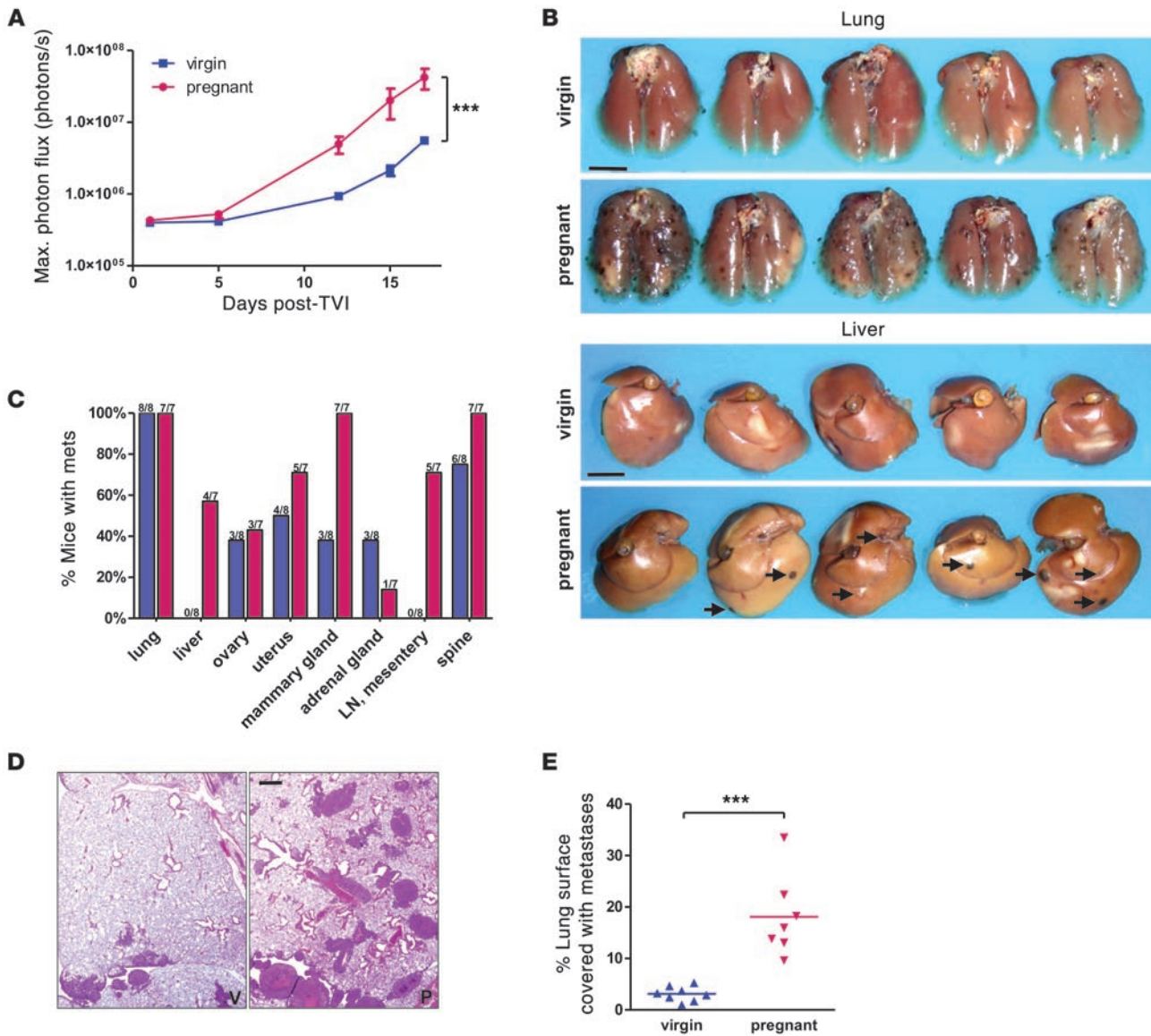


Figure 1 Pregnant mice develop more metastases upon tail vein injection (TVI) of B16.F10 cells. Luciferase-expressing B16.F10 tumor cells (5×10^5) were injected into the tail vein of 16-day pregnant and virgin NOD/SCID mice. **(A)** Evolution of the bioluminescence signal from the entire body surface of supine mice after i.p. administration of luciferin. Data are mean \pm SEM. $***P < 0.001$, 2-way repeated-measures ANOVA. **(B)** Representative macroscopic images of lung and liver metastases in formalin-fixed organs. Scale bars: 5 mm. **(C)** Organ distribution of metastases, as determined by necropsy 17 days after tumor cell injection. Blue, virgin; pink, pregnant. **(D)** Representative lung histology. Scale bar: 1 mm. P, pregnant; V, virgin. **(E)** Morphometry of lung sections (5 fields per section, 1 section per mouse). $***P < 0.001$, 2-tailed unpaired *t* test.

not been invoked in this context. Pregnancy-associated cancers (usually defined as malignancies diagnosed during pregnancy or within 1 year of parturition) do not generally differ in outcome, although there is some debate in the case of melanomas. However, the worse prognosis of pregnancy-associated breast cancer (PABC) is widely recognized but the underlying mechanisms remain obscure. Explanations including delayed diagnosis and putative tumor-promoting properties of the involuting mammary gland (19) have been proposed to result in increased stage at diagnosis. A relationship between enhanced metastatic proclivity of PABC and decreased cellular immunity has been suggested, but without firm experimental support so far (20).

A mouse model of increased experimental metastasis during gestation has been described (21), where the difference compared with nonpregnant littermates was ascribed to increased platelet-tumor cell aggregation that promotes tumor cell survival and hence enhances metastatic growth. Our present observations indicated that murine gestation augmented the rate and the degree of tumor dissemination, regardless of tumor cell origin. Moreover, we showed that decreased NK cell numbers and cytotoxicity led to blunted local clearing of tumor cells and demonstrated that MDSCs contributed to the reduced NK activity and corresponding enhancement of tumor dissemination. Furthermore, we provided evidence that pregnancy induced



metastasis-promoting changes in the lung and liver microenvironment, as revealed by the striking similarities between gene expression profiles of pregnant mouse organs and premetastatic organs in cancer-bearing mice.

Results

Pregnant mice develop a greater number of metastases than do their virgin counterparts upon i.v. injection of B16.F10 melanoma cells. B16.F10 melanoma cells were engineered to stably express firefly luciferase and were injected into the tail vein of 16-day pregnant and virgin NOD/SCID mice. Tumor cell injection around day 16 of murine gestation has previously been shown to lead to maximal enhancement of metastasis load (21). Biweekly bioluminescence imaging revealed a consistently higher tumor load in pregnant animals, culminating in 5- to 10-fold greater signal intensity than in virgin mice 17 days after tumor cell injection (Figure 1A). At this time point, mice were sacrificed, and examination at necropsy confirmed a strikingly greater tumor load in pregnant mice (Figure 1, B and C), consistent with the bioluminescence signals. In organs such as lungs that displayed metastatic colonies in both sets of animals, the size and frequency of the colonies were significantly greater in pregnant mice, as determined by quantifying metastatic lesions on lung sections (Figure 1, D and E). In addition, organs including liver and abdominal lymph nodes that were metastasis-free in virgin mice contained numerous metastases in the majority of pregnant animals (Figure 1C). Mammary glands in pregnant mice also harbored more metastases than in virgin animals, and in all organs, metastatic lesions tended to be larger in pregnant mice. Thus, the number, size, and degree of dissemination of tumor colonies were markedly increased during pregnancy.

Metastasis is enhanced in pregnant mice regardless of tumor cell type, mode of injection, and mouse strain. To determine whether the observed increase in B16.F10 cell dissemination in pregnant mice is a general or cell type-restricted phenomenon, we injected luciferase-expressing human fibrosarcoma HT1080 cells and melanoma MDA-MB-435 cells into the tail vein of virgin and 16-day pregnant immunocompromised NOD/SCID mice and assessed metastasis development over a 30- to 50-day period after injection (Figure 2, A–D, and Supplemental Figure 1, A–D; supplemental material available online with this article; doi:10.1172/JCI41936DS1). Similar to experiments using B16.F10 cells, pregnant mice bearing HT1080 and MDA-MB435 cells displayed significantly higher bioluminescence, which reflected a greater number and size of lung metastases from both cell lines. When the mouse lymphoma cell line Yac-1 was tested in experimental metastasis assays, pregnant NOD/SCID mice also had increased tumor cell load and succumbed earlier than virgin mice (Supplemental Figure 1E). Finally, tail vein injection of luciferase-expressing TA3 mouse mammary carcinoma cells into syngeneic, fully immunocompetent virgin or pregnant A/Jax mice, as well as injection of B16.F10 cells into C57BL/6 mice, attested that increased experimental metastasis in pregnant mice was not restricted to a given cell line, tumor type, mouse strain, or immunocompromised background (Figure 2, E–H, and see below).

Whereas the experimental metastasis model based on tail vein injection of tumor cells allowed demonstration of the difference in late-stage metastatic tumor growth, it did not provide evidence that development of spontaneously occurring metastases was affected. We therefore selected a model in which this issue could be addressed *in vivo*. Lewis lung carcinoma (LCC) cells were injected

s.c. into syngeneic virgin mice, and half the animals were mated within hours of injection. After 11 days, primary tumors had reached 8–9 mm in diameter and were surgically resected, and the metastasis load was monitored biweekly by bioluminescence imaging (Figure 2I). Consistent with what was observed after tail vein injection, a greater signal intensity was recorded in pregnant mice, corresponding to a larger size of lung metastases in a higher number of animals at necropsy (Figure 2, J and K). Similar results were obtained using B16.F10 cells in C57BL/6 mice (data not shown).

*Pregnancy does not affect *in vitro* and *in vivo* tumor cell growth.* To address the possible effects of pregnancy-associated circulating factors on the observed differences in tumor cell dissemination, we determined the expression of estrogen receptor (ER) and progesterone receptor (PR) on B16.F10, HT1080, MDA-MB-435, TA3, and LLC cells. Immunohistochemical analysis of lung metastases derived from the 5 cell lines failed to reveal detectable expression of either hormone receptor (Supplemental Figure 2A). We next assessed the response of the tumor cell lines to serum from virgin and pregnant NOD/SCID mice. As expected, mouse serum-stimulated cell proliferation compared to that of serum-free culture medium (Figure 3A). However, there was no significant difference between the effect of serum derived from virgin and pregnant mice in the case of B16.F10 and HT1080 cells; with MDA-MB435 and Yac-1 cells, pregnant mouse-derived serum had a weaker effect on tumor cell proliferation than did serum from virgin mice. Similar observations were made when plasma extracted from pregnant or virgin mice was used (data not shown). To compare primary tumor growth, B16.F10, HT1080, and MDA-MB435 tumor cells were injected *s.c.* into virgin and 4-day pregnant NOD/SCID mice, and tumor growth was assessed 12 days later. Similarly, *s.c.* injection of 5×10^5 LLC cells into virgin C57BL/6 mice was done immediately before breeding, and tumor growth was monitored for 11 days before resection. No significant difference was found in tumor size between pregnant and virgin animals (Figure 3B). Finally, staining of lung sections from virgin and pregnant mice 3, 6, and 10 days after tail vein injection of the MDA-MB-435 cell line failed to reveal differences in the number of cells expressing the (human) proliferation marker Ki67 (Supplemental Figure 2B). Taken together, these findings argue against a purely growth-promoting effect of pregnancy on the injected tumor cells.

Tumor cell clearance from lungs after tail vein injection is distinct in virgin and pregnant mice. Based on the observations that *in vitro* growth and *s.c.* tumor forming capacity of the cells used in these experiments were unaffected by circulating factors associated with pregnancy, we reasoned that the explanation for the observed enhancement of disseminated tumor growth in experimental metastasis assays is most likely related to changes specifically affecting circulating tumor cells or those immobilized in the target organs. To address factors that may enhance permissiveness for tumor dissemination during pregnancy, we sought to determine the time point at which a disparate evolution could first be detected, eventually leading to the massive difference in tumor load at necropsy. GFP-expressing HT1080 cells ($1-2 \times 10^6$ cells) were injected *i.v.* into virgin and 16-day pregnant NOD/SCID mice, and fluorescence stereomicroscopy was performed on lungs 1, 6, and 24 hours as well as 4 days following injection. After initially comparable lung fluorescence in both conditions, signal intensity began to diminish in virgin compared with pregnant mice as early as 6 hours after injection (Figure 4). The difference was clear at 24 hours; by 4 days, there was virtually no fluorescent signal from lungs of virgin mice, whereas the signal from lungs of pregnant mice

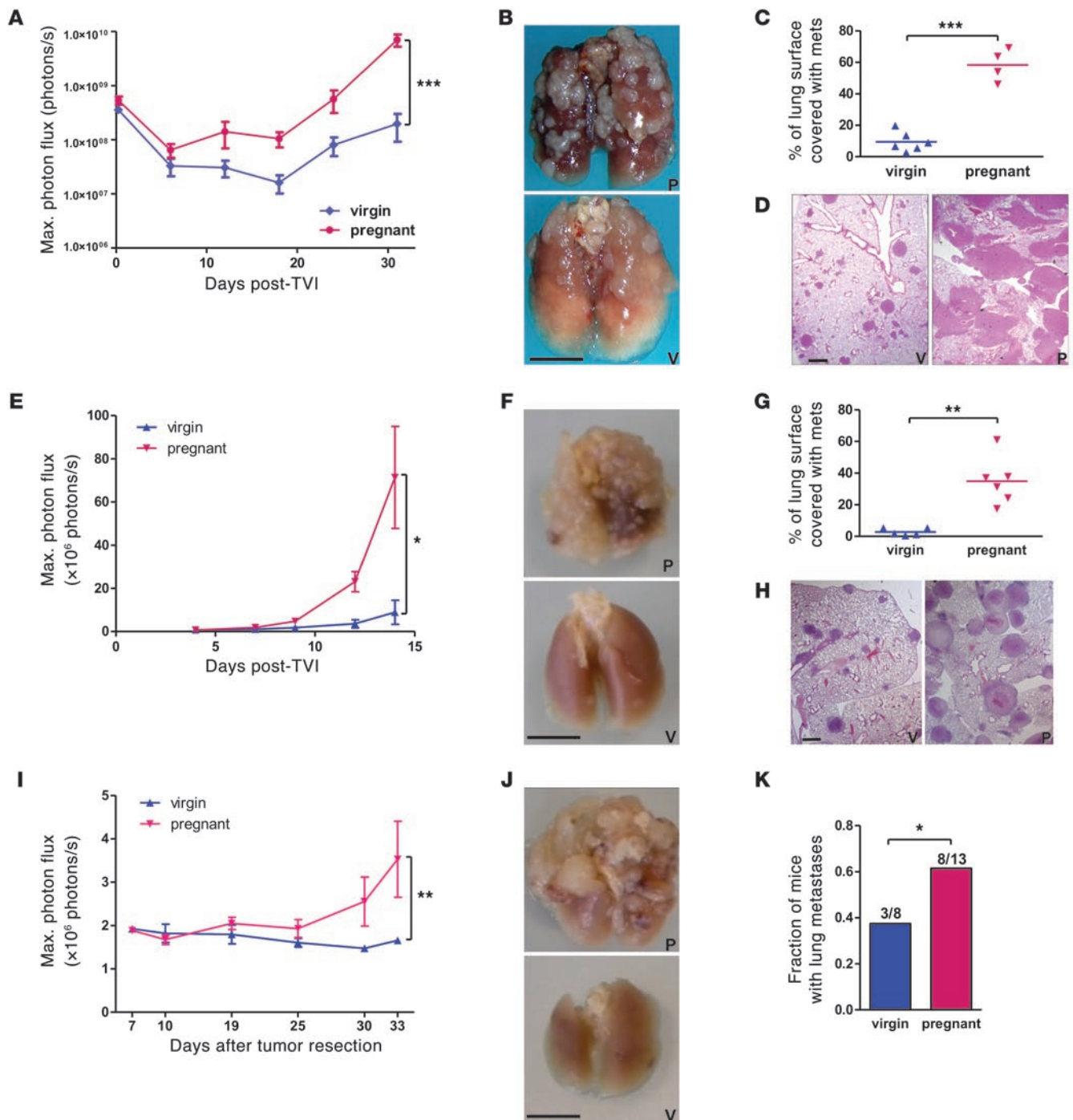


Figure 2

Increased metastasis in pregnant mice is independent of tumor cell type and mouse strain and holds true for spontaneous metastasis formation. (A–D) 7×10^5 luciferase-expressing HT1080 tumor cells were injected into the tail vein of day-16 pregnant and virgin NOD/SCID mice. (E–H) 7×10^5 luciferase-expressing TA3 tumor cells were injected into the tail vein of syngeneic day-16 pregnant and virgin A/Jax mice. (I–K) 5×10^5 luciferase-expressing LLC cells were injected s.c. into 21 virgin C57BL/6 mice, then breeding was started, yielding 13 pregnant animals. Primary tumors were resected 11 days after injection, and mice were followed up for lung metastasis development for 33 days. (A, E, and I) Evolution of the bioluminescent signal from the entire body surface of mice. * $P < 0.05$, ** $P < 0.01$, *** $P < 0.001$, 2-way repeated-measures ANOVA with Bonferroni post-test. (B, F, and J) Representative images of formalin-fixed lungs. Scale bars: 5 mm. (C and G) Histomorphometry of lung sections (4 fields per mouse). ** $P < 0.01$, *** $P < 0.001$, unpaired 2-tailed t test. (D and H) Representative lung histology. Scale bars: 1 mm. (K) Proportion of mice with macroscopic lung metastases. * $P < 0.05$, column statistics.

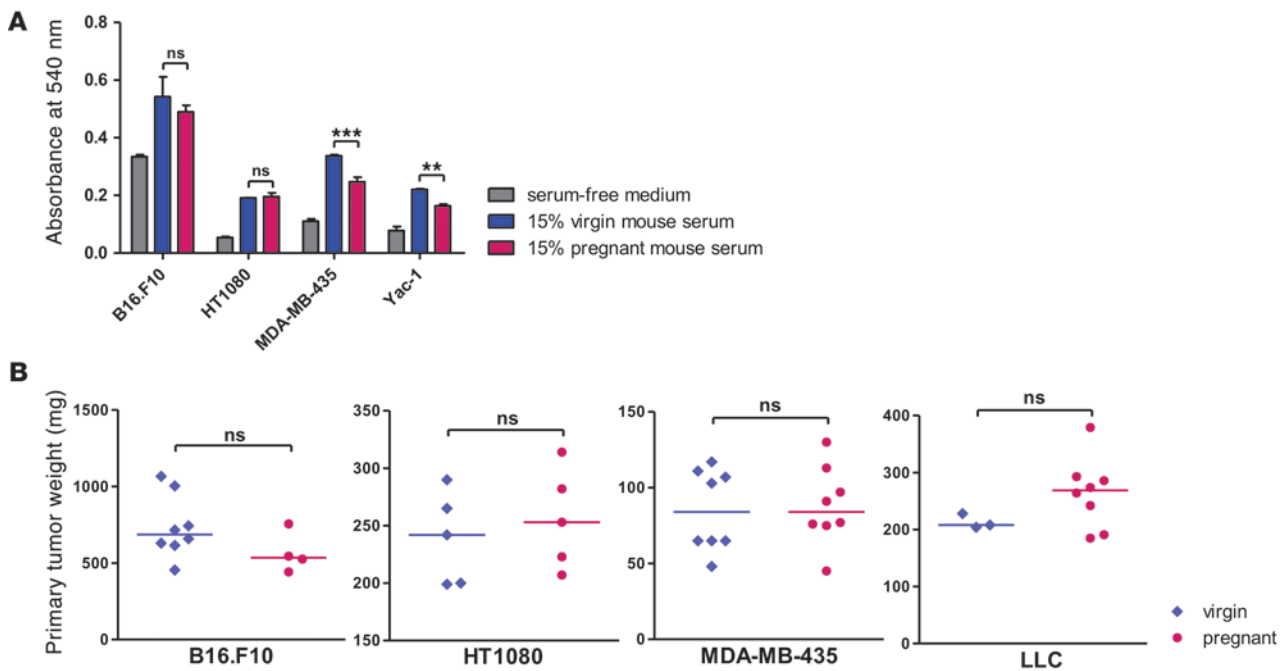


Figure 3

Gestation has no direct effect on tumor cell growth. **(A)** MTT cell proliferation assay on the indicated cells grown for 48 hours in the presence of FBS-free culture medium supplemented with 15% fresh mouse serum or plasma extracted from virgin and 16-day pregnant NOD/SCID mice. $**P < 0.01$, $***P < 0.001$. **(B)** 2×10^5 B16.F10, 7.5×10^5 HT1080, or 5×10^5 MDA-MB-435 cells were injected s.c. into 4-day pregnant and virgin NOD/SCID mice. For the experiment with LLC, 5×10^5 cells were injected into 11 virgin C57BL/6 mice, and mating was started the same day, yielding 8 pregnant mice. Tumors were resected and weighed 12 days (11 days for LLC) after injection. Horizontal bars denote medians.

displayed markedly increased intensity compared with the early time points (Figure 4). Similar, albeit not as striking, results were observed using GFP-expressing MDA-MB-435 and B16.F10 cells (Supplemental Figure 3 and data not shown). The differential decrease in the fluorescent signal emitted by pregnant and virgin mouse lungs was consistent with decreased tumor cell clearing from the lungs of pregnant mice within the first hours and days after injection.

Quantitative and qualitative changes in NK cells are responsible for increased metastatic growth in pregnant mice. The differential clearing of tumor cells from the lungs of virgin and pregnant mice prompted us to address the possible contribution of the immune system. As NOD/SCID mice are deficient in adaptive immunity, and NK cells are their first line of defense against tumor cells, we compared the number and activity of NK cells in virgin and 16-day pregnant NOD/SCID mice. Quantification was achieved by flow cytometric analysis of CD49b⁺ and NKG2D⁺ or NKp46⁺ cells (Figure 5A). Whereas NK cells represented a lower percentage of total leukocytes in the spleen and blood of pregnant mice than that in virgin mice, the proportions in lung and liver were comparable, albeit with a tendency to decrease in pregnant mice as well (Figure 5, B and C). The slight decrease of the NK cell population in the liver and lung of pregnant mice could also be appreciated on frozen sections using an anti-NKp46 antibody (Supplemental Figure 4A).

The importance of NK cell function in controlling metastasis has long been recognized (22). However, to our knowledge, no direct link has been established between decreased NK numbers and function in pregnant mice and increased experimental metastasis. We therefore investigated whether depletion of NK cells might abolish the difference in metastasis load between pregnant and

virgin NOD/SCID mice. We used 3 different strategies of NK cell depletion (Figure 5D): nonspecific leukocyte depletion by sublethal whole-body irradiation, which reduced NK cell counts in peripheral blood of virgin and 16-day pregnant NOD/SCID mice about 30-fold; specific NK cell depletion by anti-asialo GM1 (AAGM1) antibody, which resulted in a 4-fold (pregnant) to 15-fold (virgin) reduction in NK cell counts; and use of Il-2 receptor common γ subunit knockout (cg KO) NOD/SCID mice, which had no NK development at all. Upon B16.F10 tumor cell injection, the absence (cg KO mice) or near-complete depletion (irradiated mice) of NK cells resulted in overall increased metastasis take (Figure 5E), with liver metastases developing in virgin animals as well, and in the abrogation of any difference in tumor cell load between pregnant and virgin NOD/SCID mice. Consistent with this notion, virgin and pregnant cg KO NOD/SCID mice developed comparable metastatic disease upon tail vein injection of HT1080 and MDA-MB-435 tumor cells (Figure 5, F and G). Similarly, fluorescence stereomicroscopy of lungs of 16-day pregnant and virgin cg KO NOD/SCID mice at different time points after the injection of GFP-expressing HT1080 cells showed very limited tumor cell clearance from the lung microvasculature in the absence of NK cells and, more importantly, no difference between pregnant and virgin animals (Supplemental Figure 4B). However, AAGM1-treated virgin mice still developed significantly less metastases than did their pregnant counterparts, despite a greater reduction in NK numbers (Figure 5, D and E). It appears, therefore, that changes in NK cell cytotoxicity – and not merely decreased NK cell numbers – may be primarily responsible for enhanced B16.F10 metastasis in pregnant NOD/SCID mice. To determine NK activity, standard ⁵¹Cr

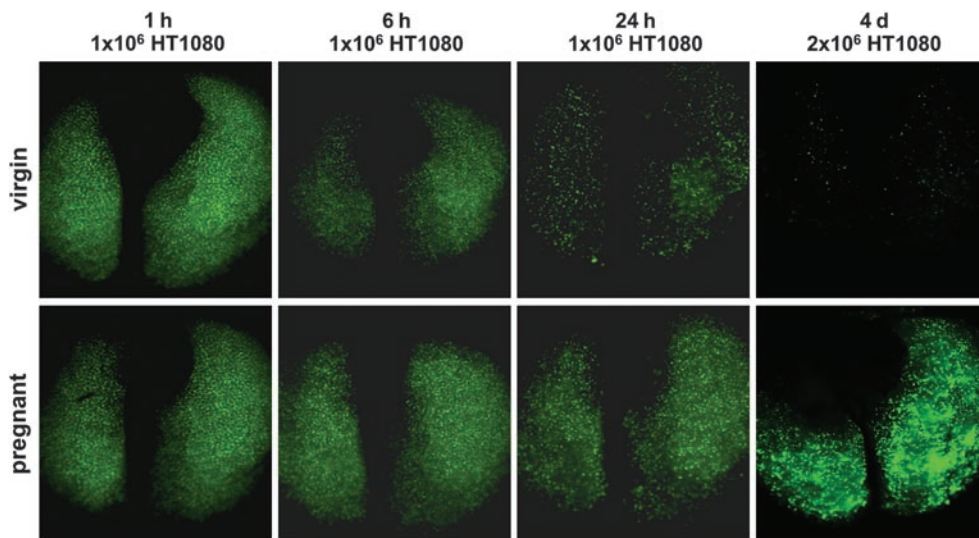


Figure 4 Differences in tumor cell load become apparent early after injection. Fluorescence stereomicroscopy of lungs at indicated time points after tail vein injection of $1\text{--}2 \times 10^6$ GFP-expressing HT1080 tumor cells into virgin and 16-day pregnant NOD/SCID mice. Exposure time was constant. Original magnification, $\times 0.71$.

release assays were performed on Yac-1 target cells using splenocytes extracted from poly(I:C)-stimulated 16-day pregnant or virgin NOD/SCID mice. Flow cytometry — adjusted for NK proportions among splenocytes — revealed an approximately 8-fold reduction in mean NK cell cytotoxicity in splenocytes derived from pregnant mice (Figure 5H). Taken together, these observations suggest that the mechanism whereby pregnancy leads to increased experimental metastasis is related to reduced NK cell-mediated clearance of tumor cells within hours of their injection.

NK cell impairment underlies increased metastasis in pregnant immunocompetent C57BL/6 mice. Whereas use of NOD/SCID mice in this experimental metastasis model had the advantage of facilitating the elucidation of the role of innate immunity in mediating increased metastasis in pregnant mice as well as allowing xenografting of human tumor cell lines, the involvement of an immune-based mechanism warranted validation in a more physiological context using immunocompetent C57BL/6 mice. Injection of syngeneic B16.F10 melanoma cells i.v. into 16-day pregnant and virgin C57BL/6 mice led to an overall higher metastasis load in pregnant animals (Figure 6A), similar to the difference observed in NOD/SCID mice.

B16.F10 melanoma cells were originally isolated from C57BL/6 mice and have been reported to be sensitive to NK cell killing. In order to address the question of how much of the difference in metastasis development can be ascribed to reduced NK function in pregnant C57BL/6 mice, we repeated the experiment with the syngeneic lymphoma cell lines RMA and EL4, which are both known to be resistant to NK cell-mediated cell cytotoxicity. The difference in metastasis take between pregnant and virgin mice was greatly reduced and did not reach statistical significance when these 2 cell lines were used (Figure 6, B and C). Nevertheless, a residual increase in tumor cell load was still apparent, possibly indicating that factors other than NK function — such as suppressed T cell activity — are implicated in increasing metastasis take in immunocompetent pregnant mice. Using flow cytometry, we found no significant difference in NK cell proportions in blood, spleen, and lung of 16-day pregnant C57BL/6 mice (Supplemental Figure 5). Decreased NK cell cytotoxicity in pregnant C57BL/6 mice was also confirmed using splenocytes in a standard ⁵¹Cr release assay (Figure 6D).

MDSC accumulation in pregnant mice contributes to increased host permissiveness to metastasis. Whereas dampened cellular immunity is an acknowledged feature of pregnancy-associated immune adaptation, little is known about how systemic NK cell function is regulated during pregnancy (17). On the other hand, MDSCs have previously been shown to inhibit NK cytotoxicity in tumor-bearing mice as well as in cancer patients (23–25). We therefore assessed whether the well-known expansion of granulocytic populations and increased leukocyte counts associated with pregnancy (26) could reflect, at least in part, the accumulation of such immunosuppressive cells. In mice, MDSCs are characterized by coexpression of CD11b and Gr-1 (27). Using flow cytometry, we found that spleen, peripheral blood, lung, and liver of pregnant NOD/SCID mice harbored significantly higher proportions of CD11b^{hi}Gr-1⁺ cells than did those derived from virgin mice (Figure 7A). Similar observations were made upon Gr-1 staining of lung and liver sections (Supplemental Figure 6A). CD11b^{hi}Gr-1^{hi} subsets constituted the major expanded fraction (Figure 7B), which could further be characterized as Ly-6C⁺Ly-6G⁺ cells (Supplemental Figure 6B). Accumulation of these cells with granulocytic morphology was also evident on blood smears and differential white blood cell counts (compare with control animals in Supplemental Figure 6I). Similarly, increased granulocyte proportions were detected in pregnant C57BL/6 mice, and CD11b^{hi}Gr-1⁺ cells — in particular, CD11b^{hi}Gr-1^{hi} fractions — accumulated in blood and spleen of these animals compared with their virgin counterparts (Supplemental Figure 6, C–E). Finally, the 3 cell populations consisting of NK, CD11b^{hi}Gr-1^{hi}, and CD11b^{hi}Gr-1^{lo} cells were monitored in the circulation throughout NOD/SCID gestation and in littermate virgin mice in parallel, beginning 3 days after mating and ending 4 days after parturition in the former, with examination of a blood sample every 3–4 days. In order to avoid confounding factors that may be caused by repetitive blood sampling in an animal, the results were expressed as a ratio of pregnant to virgin mouse cell population. MDSC (CD11b^{hi}Gr-1^{hi} more than CD11b^{hi}Gr-1^{lo}) levels rose during pregnancy, reaching a peak around day 14, and remained elevated for at least 4 days after parturition. NK levels started dropping from around day 6 of pregnancy, reaching a nadir just before parturition, and returned to normal proportions within days after giving birth (Supplemental Figure 6F).

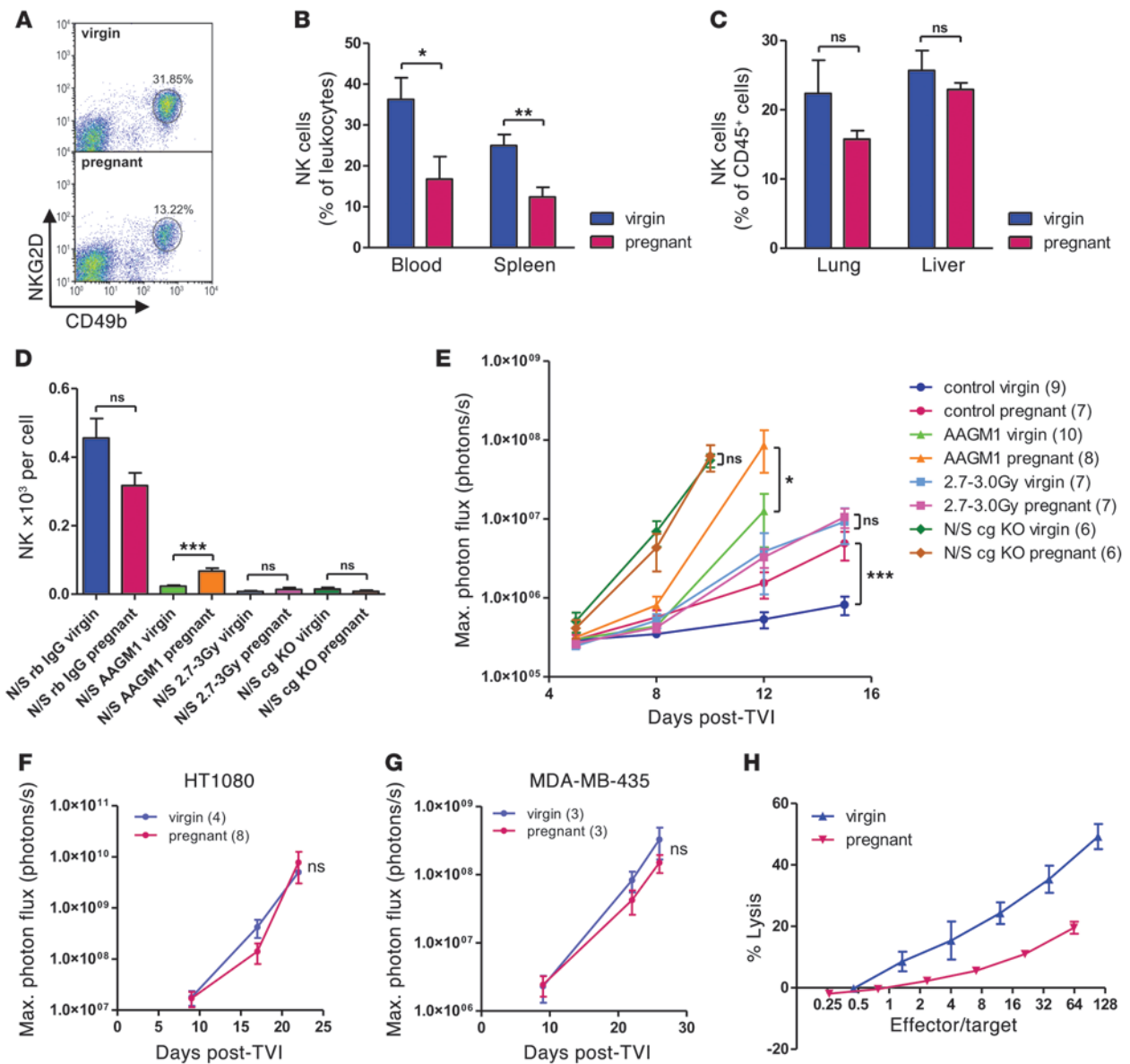
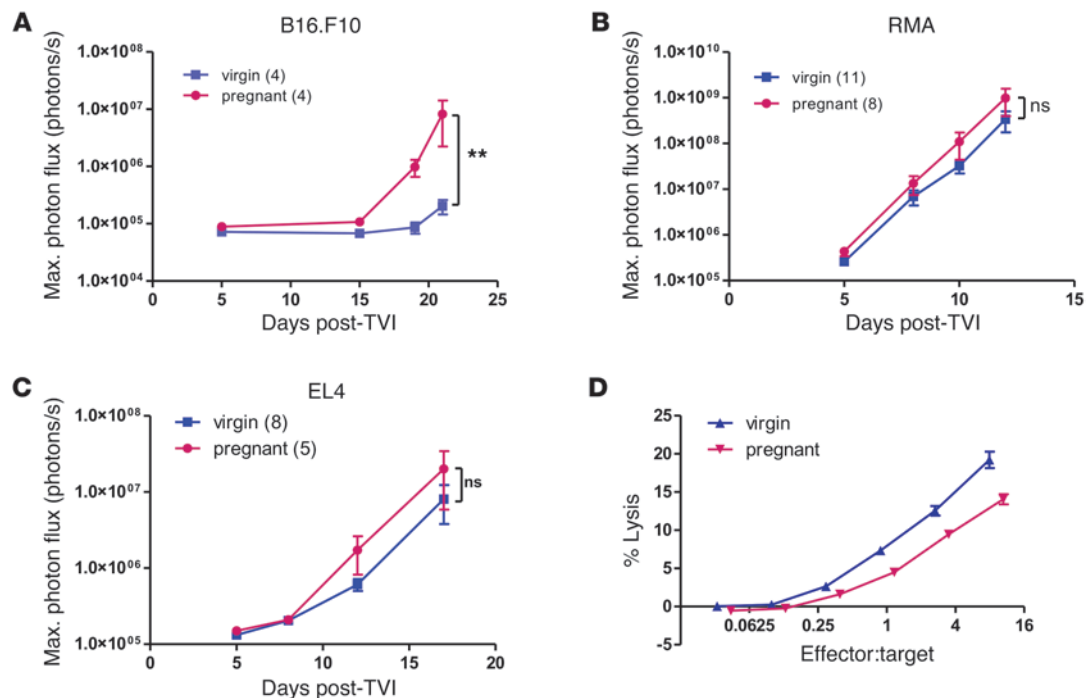


Figure 5

Quantitative and qualitative changes in NK cells are responsible for increased metastatic spread of tumors in 16-day pregnant versus virgin NOD/SCID mice. **(A)** Representative FACS images of NK cell quantification in splenocytes (CD49b⁺NKG2D⁺ in forward scatter/side scatter leukocyte gate). **(B)** Quantification of NK cells in blood and spleen by FACS analysis for CD49b⁺NKG2D⁺ cells. **P* < 0.05, ***P* < 0.01. **(C)** Quantification of NK cells in lung and liver single-cell suspensions by FACS analysis for CD49b⁺NKp46⁺ cells among CD45⁺ cells. **(D and E)** Control (rabbit IgG; rb IgG), NK-depleted (AAGM1), sublethally irradiated (2.7–3.0 Gy), and cg KO NOD/SCID mice were subjected to NK cell quantification in tail vein blood prior to tail vein injection of 1×10^5 luciferase-expressing B16.F10 tumor cells. Shown are **(D)** absolute NK numbers in tail vein blood by FACS analysis and total leukocyte counting prior to tumor cell injection and **(E)** bioluminescence imaging. Data are from 6–10 mice per condition. **P* < 0.05, ****P* < 0.001. **(F and G)** Tail vein injection of 1×10^5 luciferase-expressing HT1080 **(F)** and MDA-MB-435 **(G)** tumor cells into cg KO NOD/SCID mice and bioluminescence imaging. **(H)** Standard 4-hour ⁵¹Cr release cytotoxicity assay with splenocytes extracted from poly(I:C)-stimulated pregnant and virgin NOD/SCID mice and Yac-1 target cells. Graph was adjusted for NK proportions in splenocytes, as determined by flow cytometry. 4 mice were used per condition.

Since MDSCs are defined not only by their double-positive staining for CD11b and Gr-1, but also – and more importantly – by their functional capacity to inhibit cellular immunity and especially T cell function, we cocultured CD11b^{hi}Gr-1^{hi} cells extracted from pregnant and virgin C57BL/6 spleens using Ly-6G-coated magnetic microbeads with T cells purified from spleen

and lymph nodes of virgin C57BL/6 mice using CD90.2-coated magnetic microbeads. T cells that were in contact with Ly-6G⁺ cells from pregnant mice displayed up to 4-fold suppressed proliferation dependent on T cell/MDSC ratios, as assessed by ³H-thymidine incorporation and CFSE labeling assays (Figure 7C and Supplemental Figure 6G). Accordingly, Il-2 secretion was

**Figure 6**

NK cell impairment underlies increased metastasis in pregnant immunocompetent C57BL/6 mice. (A–C) Bioluminescence imaging after tail vein injection of 5×10^5 luciferase-expressing syngeneic, NK-sensitive B16.F10 melanoma cells (A) and NK-resistant RMA (B) and EL4 (C) lymphoma cells into 14-day pregnant and virgin C57BL/6 mice. $**P < 0.01$. (D) Standard 4-hour ^{51}Cr release cytotoxicity assay with splenocytes extracted from poly(I:C)-stimulated 16-day pregnant and virgin C57BL/6 mice and Yac-1 target cells. Graph was adjusted for NK proportions in splenocytes, as determined by flow cytometry. 4 mice were used per condition.

reduced by 30% compared with T cells that were cocultured with virgin mouse-derived Ly-6G⁺ cells (Supplemental Figure 6H). Of note, Ly-6G⁺ cells from virgin mice also suppressed proliferation and IL-2 secretion of T cells compared with T cells that had not been cocultured, albeit to a much lesser extent than pregnant mouse-derived MDSCs, suggestive of some immunoregulatory properties of Ly-6G⁺ cells derived from naive mice as well. IFN- γ was slightly diminished in T cells exposed to pregnant compared with virgin Ly-6G⁺ cells, whereas there was no difference in IL-10 production (data not shown).

We next investigated whether CD11b^{hi}Gr-1^{hi} cells contribute to reduced NK cell cytotoxicity in pregnant NOD/SCID mice. Ly-6G⁺ cells extracted from pregnant and virgin NOD/SCID splenocytes (Supplemental Figure 6B) and NK cells isolated from naive NOD/SCID female spleens using CD49b-coated magnetic microbeads were cocultured before subjecting the cell mix to standard ^{51}Cr release cytotoxicity assays using Yac-1 target cells. NK cells exposed to Ly-6G⁺ MDSCs from pregnant mice exhibited approximately 33% reduced cytotoxicity (Figure 7D).

To determine the functional effect of MDSCs on metastasis, we depleted virgin and pregnant mice of these cells using anti-Gr1 RB6-8C5 antibody. Peripheral blood smears immediately preceding B16.F10 tumor cell injection revealed robust depletion of granulocyte fractions (Supplemental Figure 6I). Injection of tumor cells after MDSC depletion resulted in unaltered metastasis in virgin mice, but significantly reduced metastasis in pregnant mouse lungs (Figure 7, E and F, and Supplemental Figure 6I). Conversely, adoptive transfer of Ly-6G⁺ spleen-derived cells prior

to Yac-1 tumor cell injection resulted in increased metastasis load in animals receiving MDSCs isolated from pregnant NOD/SCID mice compared with those receiving Ly-6G⁺ cells from virgin mice (Supplemental Figure 6K).

Gene expression profiles of pregnant and virgin mouse lung and liver reveal similarities to premetastatic niche signatures and predict outcome of patients with lung cancer. In parallel to investigating changes in the immune system that favor tumor cell dissemination during murine gestation, we sought to determine whether pregnancy also affects the target organ microenvironments, thereby generating a more metastasis-permissive “soil.” We assessed gene expression profile changes in the lung and liver of 16-day pregnant mice compared with virgin littermates using the Affymetrix mouse 430 chip. Setting the false discovery rate (FDR) at 5%, our analysis revealed up- and downregulation of 141 and 147 unique genes, respectively, in the lungs of pregnant NOD/SCID mice, and of 352 and 389 genes, respectively, in the liver of pregnant animals (Supplemental Table 1). Interestingly, of the 141 genes observed to be upregulated in pregnant mouse lungs, 13 were shared ($P = 4.1 \times 10^{-20}$, Figure 8A) with the 50 top upregulated probesets in premetastatic lungs as published by Hiratsuka et al. (10): cyclin-dependent kinase inhibitor 1A/P21 (*Cdkn1a*); cathelicidin antimicrobial peptide (*Camp*); IL-1 receptor, type II (*Il1r2*); lysyl oxidase (*Lox*); matrix metalloproteinase 8 (*Mmp8*); C-type lectin domain family 4, member d (*Clec4d*); neutrophilic granule protein (*Ngp*); S100 calcium binding protein A8/calgranulin A (*S100a8*); S100 calcium binding protein A9/calgranulin B (*S100a9*); solute carrier family 2, member 3 (*Slc2a3*); schlafen 4 (*Slf4*); elastin microfibril interfacer 2 (*Emilin2*); and cDNA sequence BC055107. The term *premetastatic niche*

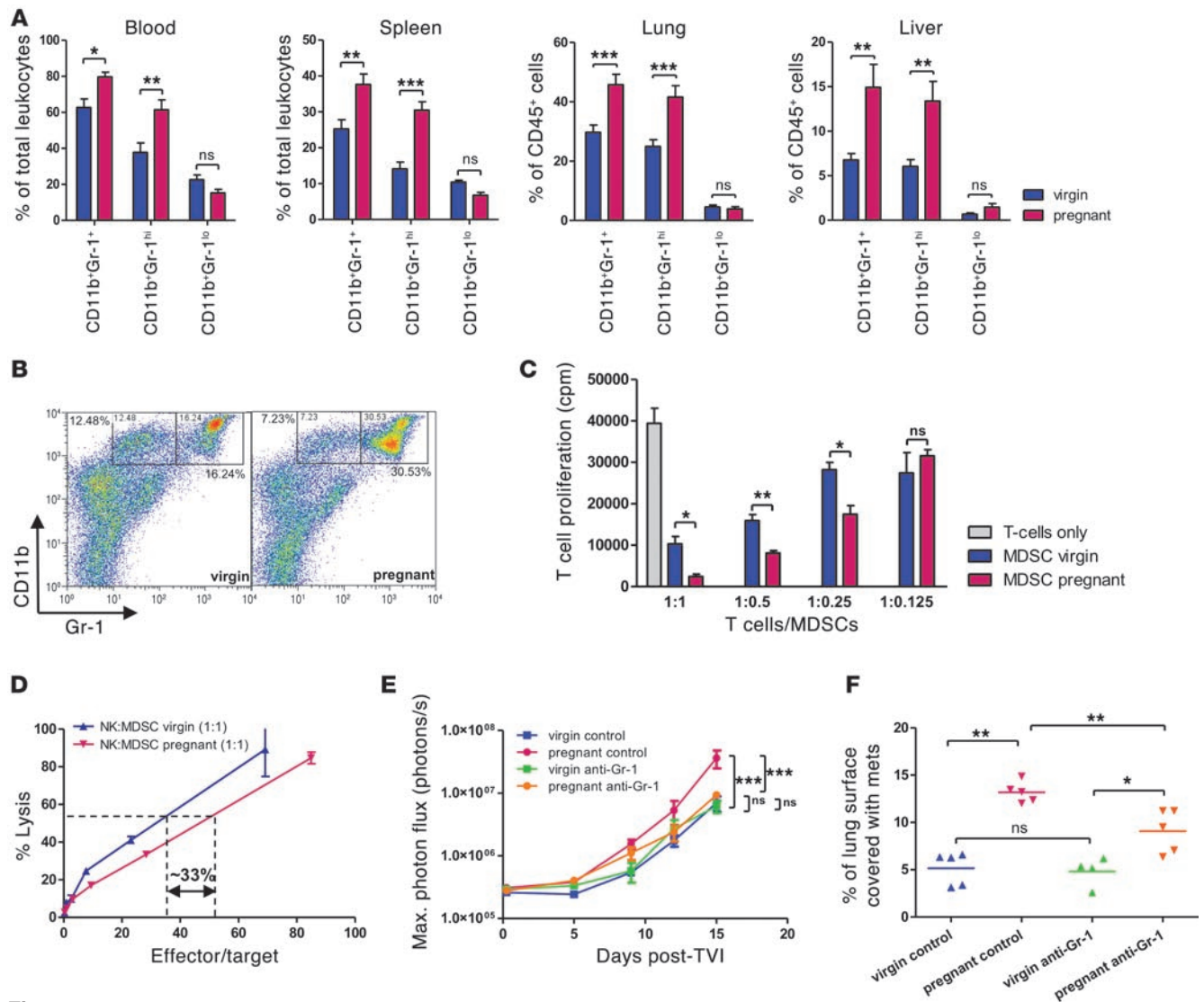
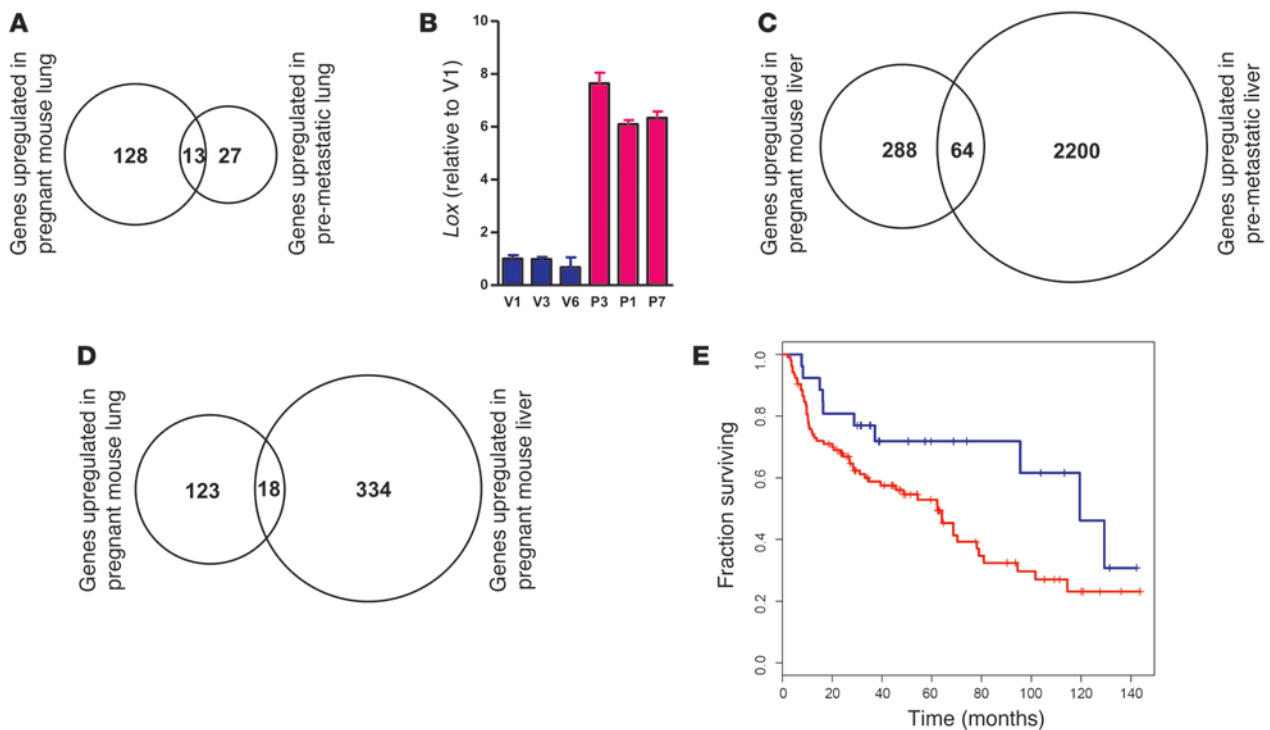


Figure 7

MDSC accumulation in 16-day pregnant mice correlates with increased permissiveness to metastasis. **(A)** Quantification of MDSCs in spleen, blood, lung, and liver of pregnant and virgin NOD/SCID mice by flow cytometry for (CD45⁺) CD11b^{hi}Gr-1⁺ cells. Overall CD11b^{hi}Gr-1⁺ cells and separate Gr-1^{hi} and Gr-1^{lo} subsets were determined. 4 mice were used per condition. **P* < 0.05, ***P* < 0.01, ****P* < 0.001. **(B)** Representative flow cytometry of spleen MDSCs. **(C)** T cell proliferation. MDSCs were isolated from splenocytes of pregnant and virgin C57BL/6 mice and T cells from virgin C57BL/6 spleen and lymph nodes by anti-Ly-6G and anti-CD90.2 magnetic beads, respectively. ³H-Thymidine incorporation assay of T cells after 3 days of MDSC coculture at the indicated ratios and in the presence of anti-CD3/anti-CD28-coated beads. **P* < 0.05, ***P* < 0.01, unpaired 2-tailed *t* test. **(D)** MDSCs were isolated from splenocytes of pregnant and virgin NOD/SCID mice and NK cells from virgin NOD/SCID spleen by anti-Ly-6G and anti-CD49b magnetic beads, respectively. ⁵¹Cr release cytotoxicity assay was performed on Yac-1 target cells after 20 hours of NK cell–MDSC coculture at a 1:1 ratio. Effector/target cell ratio was adjusted for NK proportions after coculture. **(E and F)** Tail vein injection of 5 × 10⁵ luciferase-expressing B16.F10 tumor cells after in vivo depletion of MDSCs (CD11b^{hi}Gr-1^{hi} fraction) by anti-Gr-1 antibody RB6-8C5. **(E)** Bioluminescence imaging. ****P* < 0.001. **(F)** Lung histomorphometry. **P* < 0.05, ***P* < 0.01.

has been coined to describe a situation of increased metastatic permissiveness in organs of mice bearing aggressive primary tumors. Premetastatic niches are associated with the recruitment of bone marrow–derived cells (BMDCs), which are believed to play a key role in their establishment (9, 12). Upregulated genes common to pregnant and premetastatic lungs included several that encode myeloid cell–derived proteins. *Lox*, which has been proposed to be an essential constituent of premetastatic niches (12) and is functionally involved in BMDC recruitment, displayed a robust induction in the lungs of pregnant mice as determined by quantitative RT-PCR (Figure 8B).

In parallel, gene expression profiling of pregnant mouse livers and comparative database analysis revealed significant overlaps among up- and downregulated genes in pregnant mouse liver tissue and previously described premetastatic livers from animals bearing xenotransplanted cecal tumors (ref. 28, Figure 8C, and Supplemental Figure 7A). Not surprisingly, there was a significant overlap in up- and downregulated genes between pregnant mouse lungs and liver (Figure 8D, Supplemental Figure 7B, and Supplemental Table 2), and several of the shared upregulated genes could be associated with infiltration of myeloid cells – possibly MDSCs.

**Figure 8**

Gene expression profiling of pregnant versus virgin mouse lung and comparative dataset analysis reveal similarities with a premetastatic lung signature characterized by accumulation of myelomonocytic cells. RNA from 2 mice each (16-day pregnant and virgin NOD/SCID) were pooled for 1 Affymetrix mouse 430 chip, and 3 chips were used per condition. Differentially expressed genes in the lungs and livers were determined by the rank product method by setting the false detection rate (FDR) to 5%. **(A)** Comparative analysis of upregulated genes in pregnant mouse lung with upregulated genes in premetastatic lung (mice harboring aggressive versus benign primary tumors; data derived from the heatmap of Supplemental Figure 1D in ref. 10). Overlap $P = 4.1 \times 10^{-20}$. **(B)** Quantitative RT-PCR for *Lox* in lung RNA of 16-day pregnant (P-) and virgin (V-) NOD/SCID mice. **(C)** Comparative analysis of upregulated genes in pregnant mouse liver with upregulated genes (>2 fold change) in pre-metastatic (untreated) liver (data derived from ref. 28). Overlap $P = 1.3 \times 10^{-6}$. **(D)** Commonly upregulated genes in pregnant mouse lung and liver. Overlap $P = 1.1 \times 10^{-11}$. **(E)** Unsupervised hierarchical clustering of lung cancer patients (from ref. 29) using orthologs of downregulated genes in pregnant mouse lung followed by Kaplan-Meier analysis of the 2 main patient groups (red, poor prognosis; blue, good prognosis). $P = 0.0423$. See also Supplemental Table 2.

Finally, the prognostic value of differentially expressed genes in pregnant mouse lungs was tested on lung cancer microarray data for which patient outcome was available (29). This analysis was based on the hypothesis that stromal components – including immune cells – play an important role in primary tumor progression and are represented in transcriptome analyses of bulk tumor samples. Unsupervised hierarchical clustering of lung squamous cell and adenocarcinoma gene expression data (29) revealed that the downregulated genes in pregnant mouse lungs were able to divide patients into good- and poor-prognosis groups (Figure 8E). Mean fold change of each of the 91 human orthologs of downregulated genes in pregnant mouse lungs was evaluated in both patient groups, and 51 (59%) of these genes showed lower expression levels in poor-prognosis patients ($P = 0.0046$).

Discussion

We have shown that murine gestation is associated with enhanced permissiveness for metastasis and that a candidate underlying mechanism is decreased NK cytotoxicity in the presence of an increased MDSC population. Although pregnancy, and multiple pregnancies in particular, confers protection against breast cancer

development later in life (30), breast tumors that occur during pregnancy itself or within 5 years of giving birth display a high degree of aggressiveness, with rapid dissemination and metastasis (31). Mammary gland involution has been suggested to be accompanied by tumor-promoting proinflammatory processes that could accelerate the initial steps of the metastatic cascade, including invasion and angiogenesis (32). However, pregnancy and related systemic adaptations could also contribute to increased tumor dissemination by facilitating later steps of the metastatic cascade, that is, once tumor cells have reached the lymphatic or blood circulation.

The only experimental work addressing specific metastasis-enhancing mechanisms in gestant mice has come to the conclusion that platelets from pregnant mice display greater and irreversible aggregability that increases survival of injected tumor cells and leads to greater metastasis load (21). However, adoptive transfer of platelets isolated from pregnant mice could only marginally enhance metastasis load in virgin mice (21). Accordingly, when we treated pregnant and virgin NOD/SCID mice with low-molecular weight heparin (LMWH) prior to tumor cell injection – at doses previously shown to abrogate tumor cell-induced thrombocytopenia, a measure for tumor cell-induced platelet aggregation (33) – we could only mar-



ginally decrease B16.F10 and HT1080 metastasis in pregnant mice (Supplemental Figure 8). This observation argues against a major metastasis-promoting effect of gestation-induced changes in tumor cell platelet aggregation, or the coagulation cascade, for that matter. In addition, neither serum nor plasma derived from pregnant mice had any direct positive effect on tumor cell proliferation, nor did s.c. tumors display differential growth. It therefore seemed more likely that the explanation for increased tumor dissemination during pregnancy lies in an altered tumor-host relationship. Because establishment of a relationship with host tissues that is conducive to tumor cell survival and proliferation is key for metastatic development, the observed permissiveness for tumor dissemination displayed by tissues during pregnancy may provide clues as to the identity of host factors that regulate tumor metastasis in general.

The obvious candidates among host factors that may determine metastatic tumor growth are the physical and chemical properties of tissues themselves and the state of the innate and adaptive immunity. Our observation of a rapid, but differential, clearing of tumor cells from the lung microvasculature of NOD/SCID mice, with the persistence of more tumor cells during gestation, suggests a role for innate immunity. Although immunodeficient NOD/SCID mice were used in most experiments conducted in the present study, immunodeficiency is not a prerequisite for increased metastasis in pregnant mice, since similar observations were made in fully immunocompetent A/Jax mice injected with syngeneic TA3 mammary carcinoma cells or with C57BL/6 mice challenged with B16 melanoma cells (ref. 21 and the present study). Furthermore, metastasis was also enhanced in a spontaneous metastasis assay, most likely through promotion of the late steps of the metastatic cascade. It is well established that NK cells are among the main effectors of innate antitumor immune surveillance, and their importance in controlling tumor dissemination is widely accepted (22). On the other hand, pregnancy is a state of dampened cellular immunity, and NK activity in particular has been suggested to be decreased during murine (34) as well as human (35–37) pregnancies. Accordingly, we found a decrease in NK cell proportions in blood, spleen, lungs, and liver of 16-day pregnant mice and greatly reduced NK cell cytotoxicity. The total absence of NK cells in cg KO mice or the resistance of tumor cells to NK killing abolished the difference in metastasis growth between virgin and pregnant mice. Of note, although specific — but incomplete — NK cell depletion by AAGM1 antibody increased overall metastasis load, pregnant mice still developed more metastases than did their virgin counterparts, despite the persistence of more NK cells in the former. This finding suggests that decreased NK cell effector function, rather than merely decreased NK cell numbers, is responsible for enhanced tumor dissemination. We therefore provide the first evidence to our knowledge that the pregnancy-related decrease in systemic NK cell activity is responsible for the enhancement of host permissiveness to metastasis during murine gestation and may contribute to the worse prognosis of PABC, as hypothesized previously (20).

Why systemic NK cell activity decreases during pregnancy is unclear. It is possible that NK cell function is directly affected by the increased levels of steroid hormones during pregnancy (38) or that placenta-derived microparticles (17), exosomes (39), or soluble molecules such as sHLA-G (40) regulate their activity. Alternatively, pregnancy-related circulating factors could induce immunomodulatory changes in the microenvironment of target organs of metastasis. We therefore addressed possible mechanisms by investigating transcriptome changes that occur during pregnancy. Gene expression profile analysis revealed that lungs and liver from pregnant mice bore striking

similarities to lung (10) and liver (28) premetastatic niche signatures. Commonly upregulated genes in pregnant and tumor-bearing mouse lung include *Lox* and several genes associated with myeloid cell recruitment. LOX is secreted by hypoxic breast tumors and accumulates in the lungs of tumor-bearing animals prior to tumor cell dissemination, where it modifies basement membranes and contributes to BMDC recruitment (12, 41). Primary tumors are known to elaborate soluble factors (i.e., TDSFs) that drive the formation of privileged sites for the engraftment of disseminating tumor cells; moreover, TDSFs have been shown to orchestrate the expansion and activation of myeloid cell precursors that display suppressive activity for both adaptive and innate immunity (16). These MDSCs are characterized by double-positive CD11b and Gr-1 staining in mice and accumulate in the primary tumor, tumor-draining lymph nodes, spleen, and lung of tumor-bearing animals. However, they have not been suggested to be constituents of premetastatic niches.

Premetastatic niches are characterized by the accumulation of BMDCs (42) that have further been characterized as CD11b⁺ cells (9, 10, 12) or Gr-1⁺ cells (28). To our knowledge, no experimental work thus far has shown an immunosuppressive function of these myeloid cells recruited to premetastatic sites, although a recent review raises the point that BMDCs may create “immune sanctuary sites” that favor survival and proliferation of engrafted metastatic cells (8). We provide evidence that CD11b^{hi}Gr1⁺ cells — in particular CD11b^{hi}Gr-1^{hi} subsets — accumulate in pregnant mouse blood, spleen, lung, and liver, raising the possibility that the corresponding immunosuppressive activity may have a blunting effect on NK cell function. The anti-Gr-1 antibody recognizes 2 distinct epitopes: Ly-6C, expressed on Gr-1^{lo} cells; and Ly-6G, expressed on the Gr-1^{hi} population. Gr-1^{hi} cells of granulocytic morphology isolated from pregnant mice using anti-Ly-6G magnetic microbeads inhibited T cell proliferation and Il-2 secretion in addition to decreasing NK cell cytotoxicity *in vitro* compared with cells extracted from their virgin counterparts. This immunosuppressive function strongly supports the notion that the myeloid cells accumulating during murine gestation are indeed MDSCs. Consistent with these observations, MDSCs isolated from tumor-bearing animals have been shown to decrease NK activity in a cell contact-dependent manner and to be responsible for increased tumor dissemination (24, 25).

Finally, the observation that *in vivo* depletion of MDSCs using anti-Gr-1 antibody reduced metastatic tumor spread in pregnant mice, but not in virgin mice, confirms their mechanistic involvement in enhancing permissiveness to metastasis in pregnant mice. This finding and the results of the adoptive transfer experiment lend further support to the notion that Gr-1⁺ cells are functionally distinct in pregnant and virgin animals. This is in accordance with several reports that show immunosuppressive function of CD11b^{hi}Gr1⁺ cells derived from tumor-bearing, but not tumor-free, mice (24, 43).

Comparative analysis of differentially expressed genes of pregnant mouse lungs and liver and of premetastatic niches in organs of tumor-bearing mice (10, 28) revealed the upregulation of *S100a8* and *S100a9* in all 4 gene expression profiles, representing situations of enhanced metastatic growth. Hiratsuka and colleagues have shown how these chemoattractants produced by cells of the myeloid lineage not only recruit additional BMDCs, but also attract circulating tumor cells and enhance their invasiveness, thereby favoring lung colonization (10, 11). On the other hand, these chemotactic molecules are important inflammatory mediators that have been shown to contribute to MDSC accumulation and function in primary tumors (44, 45). The combined findings of *S100a8* and *S100a9*



upregulation and MDSC accumulation in pregnant mouse lungs and liver further validate the hypothesis that MDSCs may participate in the elaboration of the premetastatic niche, thereby not only facilitating tumor progression at the primary site, but also enhancing the establishment of metastatic lesions.

In a clinical study, MDSC numbers have been shown to correlate with cancer stage and to influence prognosis (46). As the gene expression profile of pregnant mouse lung is suggested to reflect the accumulation of these cells, we addressed the possibility that our differentially expressed genes could be found in the stromal component of lung cancers and, when present, could correlate with worse outcome. Kaplan-Meier survival analysis of lung squamous cell and adenocarcinoma patients clustered into 2 groups according to expression of downregulated genes in pregnant mouse lung indicated that our signature performs well in predicting outcome. This observation is consistent with our previous work on a purely stromal cell-derived signature associated with invasive prostate cancer that was able to segregate primary prostate cancer samples with good prognosis from those with poor prognosis (47). Analysis of mean fold change in lung cancer samples revealed that the majority of downregulated genes in pregnant mouse lung were also less expressed in samples of patients clustering into the poor-prognosis group, which suggests that these genes may have metastasis and primary tumor suppressor functions when expressed by stromal cells.

In conclusion, we postulate that the many previously reported similarities in molecular and cellular mechanisms involved in cancer progression and placentation (48) should be extended to include a common mechanism for increasing permissiveness to metastasis in target organs by a process that involves, at least in part, accumulation of MDSCs and suppression of NK cell activity. MDSC accumulation has not to our knowledge been invoked previously in the context of pregnancy, but may well be a means whereby uterine as well as systemic maternal immune tolerance are regulated.

Methods

Animals. Female standard and cg KO NOD/SCID mice were obtained from in-house breeding at the ISREC mouse facility. C57BL/6 mice were from Jackson Laboratories, A/JOIaHsd mice from Harlan Laboratories. Female mice were between 8 and 10 weeks old at the beginning of experiments. Pregnancy was timed by checking for vaginal plugs early mornings for 4 days after setting up breeding couples. Experiments involving mice were approved by the Etat de Vaud, Service Vétérinaire (Epalinges, Switzerland; authorization no. VD1477.1)

Reagents. The antibodies used were as follows: anti-ER MAb (RTU-ER-6F11) from Novocastra; anti-PR MAb (PgR 63) and anti-human Ki67 MAb (M7240) from DakoCytomation; anti-GFP MAb (11 814 460 001) from Roche; rat anti-mouse CD11b-PE (M1/70), hamster anti-mouse CD49b-PE (HM α 2), rat anti-mouse CD16/32 (2.4G2), rat anti-mouse IL-2 (clone JES6-5H4), rat anti-mouse IL-10 (JES5-16E3), and rat anti-mouse IFN- γ (XMG1.2) from BD Biosciences – Pharmingen; rat anti-mouse NKG2D-APC (CX5), rat anti-mouse NKp46-Alexa Fluor 647 (29A1.4), and mouse anti-mouse NK1.1-APC (PK136) from eBioscience; rat anti-mouse CD45-PE-Cy7 (30-F11) from BioLegend; rat anti-mouse Gr-1-FITC (Ly-6G/Ly-6C; RB6-8C5) from BioLegend and BioXCell (for in vivo depletion); rabbit AAGM1 from WAKO; and appropriate isotype controls and HRP-conjugated secondary antibodies. poly(I:C) was from Sigma-Aldrich. D-luciferin (firefly) potassium salt was from Biosynth. MACS cell sorting reagents were as follows: anti-CD49b-conjugated magnetic microbeads (DX5) and biotinylated anti-Ly-6G (1A8) antibody with anti-biotin-conjugated magnetic microbeads (Miltenyi Biotec). Collagenase II from *Clostridium*

histolyticum was from Sigma-Aldrich. Recombinant human IL-2 was from ImmunoTools. Baytril antibiotics, 10% oral solution, were from Bayer.

Luciferase and GFP transduction of tumor cells. cDNA encoding firefly luciferase (from pGL3) and enhanced GFP were cloned into second-generation lentivectors containing a EF1 α or CMV promoter and puromycin or hygromycin selection markers. B16.F10, LLC, TA3, HT1080, and MDA-MB-435 cells were cultured in DMEM supplemented with 10% FBS. RMA, EL4, and Yac-1 cells were maintained in RPMI-1640 supplemented with 10% FBS.

Tumor cell injection, tumor resection, and adoptive transfer of MDSCs. For tail vein or s.c. injections, subconfluent tumor cells were detached with EDTA, washed, and resuspended in DMEM. For spontaneous metastasis assay, primary tumors (8–9 mm largest diameter) were resected 11 days after s.c. injection under general anesthesia. For MDSC adoptive transfer, cells were isolated with anti-Ly-6G microbeads, washed in PBS, and injected (6×10^6 cells per animal) into the tail vein 20 hours prior to tumor cell injection. At least 5 animals per condition were used. Results shown are representative of at least 2 independent experiments.

Sublethal irradiation and NK cell and MDSC depletion. Sublethal γ irradiation of virgin and 14-day pregnant NOD/SCID mice was performed using a ^{137}Cs source (1.6 Gy/min), and irradiation time was adjusted to reach a total dose of 2.7–3.0 Gy per animal. For NK cell depletion, rabbit AAGM1 (~400 μg) was injected i.v. 4 and 2 days prior to B16.F10 tail vein injection. Depletion efficiency was tested by flow cytometry of blood samples. For MDSC depletion, anti-Gr-1 antibody (RB6-8C5; 250 μg per injection) was injected into the tail vein of virgin and pregnant mice, 3 and 1 days prior to tumor cell injection and 1 day later. Depletion efficiency was assessed on blood smears. For NK cell and MDSC depletion, appropriate control Igs – rabbit IgG and rIgG_{2b} (clone LTF2), respectively – were injected into control animals. All animals were given antibiotic prophylaxis (300 μl Baytril in 250 ml drinking water).

Immunohistochemistry, lung histomorphometry, and blood leukocyte enumeration. Formalin-fixed, paraffin-embedded lung tissue was stained for GFP, hKi67, ER, and PR according to the manufacturer's recommendations. H&E staining was done according to standard procedures. 4–5 fields of 1 H&E-stained lung section per animal were photographed at $\times 20$ magnification, and the percentage of lung surface occupied by metastatic lesions was determined as a pixel ratio in Photoshop CS. For quantification of leukocytes, mouse blood (cardiac or tail vein) was collected into 1.2 ml EDTA monovette tubes (Sarstedt) and diluted 1:20 in Leukoplate (SOBODIA) before counting in a Neubauer chamber. Blood smears were stained with Giemsa-Wright (HemoQuick; Labo Moderne).

Mouse serum and plasma extraction and proliferation assay. Blood was obtained from pregnant and virgin mice by cardiac puncture. For serum extraction, whole blood was left to coagulate at room temperature for 15 minutes, then spun at 1,000 g for 15 minutes. For plasma preparation, blood was collected in a syringe containing 10 IE liqemim (Roche), diluted 1:1 with serum-free medium, and then spun at 1,500 g for 15 minutes. 3×10^3 B16.F10, HT1080, and MDA-MB-435 cells were seeded into wells of a 96-well plate 24 hours before the assay and serum-starved overnight. Mouse serum and plasma were diluted to 15% in serum-free medium and added to the tumor cells. MTT assay (Promega) was performed according to the product protocol after 48 hours of incubation. Serum from 3 different mice was used per condition, and the experiment was conducted in triplicates for each cell line and serum. Plasma was prepared from 1 mouse per condition in duplicate wells.

Fluorescence stereomicroscopy. Mouse lungs were excised at given time points after tail vein injection of GFP-expressing tumor cells and immediately visualized under a Leica MZ16 1FA fluorescence stereomicroscope with a fixed exposure time to compare pictures from pregnant and virgin mouse lungs.

In vivo bioluminescence imaging. After tail vein injection of luciferase-expressing tumor cells, total tumor cell load was assessed at various intervals by bioluminescence imaging in an IVIS 200 series system (Xenogen) after i.p. luciferin



administration (75 mg/kg) and under isoflurane anesthesia. Several images over a 10- to 20-minute period were taken, and maximal photon flux over the whole body area was determined using Living Image Software (Xenogen).

Cell harvesting for cytotoxicity assays, flow cytometry, and cell isolation. Where indicated, mice were stimulated with 100 µg poly(I:C) i.p. 36 hours prior to splenocyte extraction. Virgin or 16-day pregnant NOD/SCID mice were sacrificed by cervical dislocation, and the heart was punctured for blood collection into a 1.2-ml monovette (EDTA anticoagulation). Blood leukocytes were prepared by ammonium chloride buffer erythrolysis. Splenocytes were prepared by pressing the spleen through a 70-µm nylon mesh (BD Falcon). Platelets were removed by 2 rounds of slow spinning in PBS (300 g for 10 minutes). For flow cytometry and magnetic bead cell sorting (MACS), splenocyte suspensions were filtered through single-cell strainers. Lung and liver were minced with a razor blade prior to digestion in collagenase II (5 mg in 5 ml RPMI-1640 with 10% FBS for 1 hour at 37°C), and single-cell suspensions were obtained after sieving through a single-cell strainer.

⁵¹Cr release cytotoxicity assay. Splenocytes were harvested from pregnant and virgin mice as described above, and ⁵¹Cr release assays were performed according to standard procedures. 10⁶ Yac-1 cells were washed in complete medium and incubated with 50–100 µl Na₂⁵¹CrO₄ for 1 hour at 37°C. Labeled cells were washed in complete medium and aliquoted into wells containing splenocytes (1,000 Yac-1 cells/well). After 4 hours of incubation at 37°C, ⁵¹Cr release into the media was quantified using LumaPlate-96 plates (Perkin-Elmer) and a Top-Count-γ-counter (PerkinElmer). 0% lysis was determined with complete medium only, 100% lysis by adding 100 µl of 1 M HCl to the target cells. Percent lysis was determined as (sample lysis – 0% lysis)/(100% lysis – 0% lysis). NK cell proportions of each sample were determined by flow cytometry, and effector/target ratios were adjusted accordingly.

NK cell, T cell, and MDSC isolation. NK cells, T cells, and MDSCs were isolated from virgin and 16-day pregnant NOD/SCID splenocytes (and lymph nodes for T cells) according to the manufacturer's recommendations. Briefly, erythrocyte-free single-cell suspensions (typically ~1 × 10⁸ cells per condition) were washed and resuspended in MACS buffer and anti-CD49b-conjugated (NK cell isolation), anti-CD90.2-conjugated magnetic beads (T cell isolation), or biotinylated anti-Ly-6G antibody (MDSC isolation) mix and processed according to the manufacturer's recommendations prior to separation on LS columns in a magnet (Miltenyi Biotec).

NK cell–MDSC coculture. MACS-isolated NK cells from 3–5 virgin NOD/SCID spleens and MDSCs extracted from 3–5 virgin and 3–5 pregnant mouse spleens were mixed at a 1:1 ratio (typically 1 × 10⁶ cells each) and cocultured for 20 hours in RPMI-1640 plus 10% FBS and 250 ng/ml recombinant human IL-2 in a 24-well plate. Cells were aliquoted in triplicates into 96-well plates for ⁵¹Cr release cytotoxicity assay on Yac-1 target cells. Viability was assessed by trypan blue exclusion, and NK cell proportion was redetermined by flow cytometry after coculture.

T cell–MDSC coculture. MACS-isolated T cells from virgin NOD/SCID spleens and MDSCs from virgin and pregnant mouse spleens and lymph nodes were mixed at several ratios and cocultured in RPMI-1640 plus 10% FBS in a 96-well plate in the presence of anti-CD3/anti-CD28-coated beads (DynaL Biotech) at a 1:1 ratio for T cell stimulation. For ³H-thymidine proliferation assays, ³H-T was added (1 curie/well) after 3 days of co-culture, and the plate was read 18 hours later in a Top-Count-γ-counter (PerkinElmer). For the CFSE proliferation assay, T cells were incubated in 1 ml of 2 µM CFSE solution (eBioscience) for 15 × 10⁶ cells, 10 minutes at 37°C, before the coculture with virgin or pregnant MDSC. 4 days later, cells were analyzed by flow cytometry.

Flow cytometry. Blood leukocytes and single-cell suspensions from spleen, lung, and heart were prepared as described above. 10⁶ cells were aliquoted into 5-ml tubes and washed with FACS buffer (PBS plus 3% FBS and 0.9% NaN₃). Cells were preincubated with anti-CD16/CD32 and 2% goat serum for 10 minutes at 4°C. Staining was done for 30–45 minutes at 4°C. Antibody

dilutions were as follows: CD45-PE-Cy7 (1:200), CD11b-PE (1:400), Gr-1-FITC (1:300), CD49b-PE (1:400), NKp46-Alexa Fluor 647 (1:200), NKG2D-APC (1:200), NK1.1-APC (1:200). Intracellular levels of T cell cytokines were assessed upon a 4-day T cell–MDSC coculture: 4 × 10⁶ T cells were restimulated with 1 ml of 50 ng/ml PMA, 0.5 µg/ml ionomycin, and 10 µg/ml brefeldin A (all from Sigma-Aldrich) for 4 hours at 37°C. Cells were then permeabilized with FACS buffer plus 0.5% saponin before staining with IFN-γ-PE (1:200), IL-2-APC (1:100), and IL-10-PE (1:200) antibodies and flow cytometry analysis on a FACSCalibur apparatus (BD), and FlowJo software (Tree Star Inc.) for image analysis and quantification of cell populations.

Affymetrix gene expression profiling and comparative analyses. Lungs and livers of pregnant and virgin mice were ground in liquid nitrogen and the powder homogenized by resuspension in RLT lysis buffer. RNA extraction was done using Qiagen RNeasy Kit according to the manufacturer's recommendations. Total RNA quality was verified by an Agilent RNA 600 nanoassay. cRNA synthesis, hybridization to an oligonucleotide array (GeneChip Mouse Expression Set 430; Affymetrix), and scanning were done by the DNA Array Facility of the University of Lausanne (DAFL). 3 chips were done per organ and per condition, with equal amounts of RNA from 2 mice pooled per chip. Normalization and background subtraction were performed with RMA (49), using the “affy” library (50) of Bioconductor (51). Differentially expressed genes were determined using rank-products (52), specifically the Bioconductor package RankProd (53). Statistical significance of the overlaps with published gene signatures was computed with a 1-tailed exact Fisher's test with Bonferroni correction where multiple testing was performed. Microarray data were deposited in GEO (accession no. GSE18907).

Quantitative real-time PCR. cDNA was obtained using MMLV reverse transcriptase and RNase H minus (Promega). Real-time PCR amplification was done using specific intron spanning primers and appropriate Universal Probe library probe for Lox in an ABI Prism 7700 instrument (Applied Biosystems). Relative quantification of target, normalized with an endogenous control (18s), was done using a comparative Ct method.

Statistics. Graphs and statistics were done using GraphPad Prism 5.0 software. Mean ± SEM is depicted in all graphs. Statistical significance was determined by 2-way ANOVA for repeated measurements with Bonferroni post-test for bioluminescence data; by unpaired 2-tailed *t* test for lung histomorphometry, primary tumor weight, MTT assay, and flow cytometry results comparing 2 groups; and by 1-way ANOVA with Bonferroni post-test for lung histomorphometry comparing 4 groups. A *P* value less than 0.05 was considered significant.

Acknowledgments

We are indebted to Marina Bacac, Carlo Fusco, and Roland Meier for invaluable discussions and critical reading of the manuscript. The help and suggestions of Werner Held and Pedro Romero regarding NK experiments are gratefully acknowledged. We also thank Cynthia Dayer for help with fluorescence stereomicroscopy. L.A. Mauti was supported by a MD-PhD grant from the Swiss National Foundation. This work was supported by Swiss National Science Foundation grant 31003A-105833 and the NCCR Molecular Oncology (to I. Stamenkovic).

Received for publication December 3, 2009, and accepted in revised form April 20, 2011.

Address correspondence to: Ivan Stamenkovic, Division of Experimental Pathology, Institute of Pathology, Centre Hospitalier Universitaire Vaudois (CHUV), Rue du Bugnon 25, 1005 Lausanne, Switzerland. Phone: 41.21.314.7136; Fax: 41.21.314.7110; E-mail: Ivan.Stamenkovic@chuv.ch.



1. Gupta GP, Massague J. Cancer metastasis: building a framework. *Cell*. 2006;127(4):679–695.
2. Weiss L. Metastatic inefficiency. *Adv Cancer Res*. 1990;54:159–211.
3. Luzzi KJ, et al. Multistep nature of metastatic inefficiency: dormancy of solitary cells after successful extravasation and limited survival of early micro-metastases. *Am J Pathol*. 1998;153(3):865–873.
4. Nieswandt B, Hafner M, Echtenacher B, Man- nel DN. Lysis of tumor cells by natural killer cells in mice is impeded by platelets. *Cancer Res*. 1999;59(6):1295–1300.
5. Aguirre-Ghiso JA. Models, mechanisms and clinical evidence for cancer dormancy. *Nat Rev Cancer*. 2007;7(11):834–846.
6. Teng MW, Swann JB, Koebel CM, Schreiber RD, Smyth MJ. Immune-mediated dormancy: an equilibrium with cancer. *J Leukoc Biol*. 2008;84(4):988–993.
7. Khatami M. Inflammation, aging, and cancer: tumoricidal versus tumorigenesis of immunity: a common denominator mapping chronic diseases. *Cell Biochem Biophys*. 2009;55(2):55–79.
8. Psaila B, Lyden D. The metastatic niche: adapting the foreign soil. *Nat Rev Cancer*. 2009;9(4):285–293.
9. Kaplan RN, et al. VEGFR1-positive haematopoietic bone marrow progenitors initiate the pre-metastatic niche. *Nature*. 2005;438(7069):820–827.
10. Hiratsuka S, Watanabe A, Aburatani H, Maru Y. Tumour-mediated upregulation of chemoat- tractors and recruitment of myeloid cells predetermines lung metastasis. *Nat Cell Biol*. 2006;8(12):1369–1375.
11. Hiratsuka S, et al. The S100A8-serum amyloid A3-TLR4 paracrine cascade establishes a pre-metastatic phase. *Nat Cell Biol*. 2008;10(11):1349–1355.
12. Erler JT, et al. Hypoxia-induced lysyl oxidase is a critical mediator of bone marrow cell recruit- ment to form the premetastatic niche. *Cancer Cell*. 2009;15(1):35–44.
13. Taranova AG, et al. Allergic pulmonary inflammation promotes the recruitment of circulating tumor cells to the lung. *Cancer Res*. 2008;68(20):8582–8589.
14. Dunn GP, Old LJ, Schreiber RD. The immunobiology of cancer immunosurveillance and immunoed- iting. *Immunity*. 2004;21(2):137–148.
15. Ostrand-Rosenberg S, Sinha P. Myeloid-derived suppressor cells: linking inflammation and cancer. *J Immunol*. 2009;182(8):4499–4506.
16. Gabrilovich DI, Nagaraj S. Myeloid-derived sup- pressor cells as regulators of the immune system. *Nat Rev Immunol*. 2009;9(3):162–174.
17. Sargent IL, Borzychowski AM, Redman CW. NK cells and human pregnancy—an inflammatory view. *Trends Immunol*. 2006;27(9):399–404.
18. Trowsdale J, Betz AG. Mother's little helpers: mech- anisms of maternal-fetal tolerance. *Nat Immunol*. 2006;7(3):241–246.
19. Schedin P. Pregnancy-associated breast cancer and metastasis. *Nat Rev Cancer*. 2006;6(4):281–291.
20. Shakhar K, Valdimarsdottir HB, Bovbjerg DH. Heightened risk of breast cancer following preg- nancy: could lasting systemic immune altera- tions contribute? *Cancer Epidemiol Biomarkers Prev*. 2007;16(6):1082–1086.
21. Tanaka H, et al. Increased experimental pulmo- nary metastasis in pregnant mice. *Int J Cancer*. 1995;62(3):314–318.
22. Hanna N. Role of natural killer cells in control of cancer metastasis. *Cancer Metastasis Rev*. 1982; 1(1):45–64.
23. Hoehchst B, et al. Myeloid derived suppressor cells inhibit natural killer cells in patients with hepatocellular carcinoma via the NKP30 receptor. *Hepatol- ogy*. 2009;50(3):799–807.
24. Li H, Han Y, Guo Q, Zhang M, Cao X. Cancer- expanded myeloid-derived suppressor cells induce anergy of NK cells through membrane-bound TGF-beta 1. *J Immunol*. 2009;182(1):240–249.
25. Liu C, et al. Expansion of spleen myeloid suppres- sor cells represses NK cell cytotoxicity in tumor- bearing host. *Blood*. 2007;109(10):4336–4342.
26. Kuhner M, Strohmeier R, Stegmuller M, Halber- stadt E. Changes in lymphocyte subsets during normal pregnancy. *Eur J Obstet Gynecol Reprod Biol*. 1998;76(2):147–151.
27. Serafini P, Borrello I, Bronte V. Myeloid suppressor cells in cancer: recruitment, phenotype, properties, and mechanisms of immune suppression. *Semin Cancer Biol*. 2006;16(1):53–65.
28. Yamamoto M, et al. TSU68 prevents liver metastasis of colon cancer xenografts by modulating the pre- metastatic niche. *Cancer Res*. 2008;68(23):9754–9762.
29. Raponi M, et al. Gene expression signatures for pre- dicting prognosis of squamous cell and adenocarcino- mas of the lung. *Cancer Res*. 2006;66(15):7466–7472.
30. Russo J, Moral R, Balogh GA, Mailo D, Russo IH. The protective role of pregnancy in breast cancer. *Breast Cancer Res*. 2005;7(3):131–142.
31. Lyons TR, Schedin PJ, Borges VF. Pregnancy and breast cancer: when they collide. *J Mammary Gland Biol Neoplasia*. 2009;14(2):87–98.
32. McDaniel SM, et al. Remodeling of the mam- mary microenvironment after lactation promotes breast tumor cell metastasis. *Am J Pathol*. 2006; 168(2):608–620.
33. Mousa SA, Linhardt R, Francis JL, Amirkhosravi A. Anti-metastatic effect of a non-anticoagulant low-molecular-weight heparin versus the standard low-molecular-weight heparin, enoxaparin. *Thromb Haemost*. 2006;96(6):816–821.
34. Furukawa K, Itoh K, Okamura K, Kumagai K, Suzuki M. Changes in NK cell activity during the estrous cycle and pregnancy in mice. *J Reprod Immunol*. 1984;6(6):353–363.
35. Baley JE, Schacter BZ. Mechanisms of diminished natural killer cell activity in pregnant women and neonates. *J Immunol*. 1985;134(5):3042–3048.
36. Gabrilovac J, Zadjelovic J, Osmak M, Suchanek E, Zupanovic Z, Boranic M. NK cell activity and estrogen hormone levels during normal human preg- nancy. *Gynecol Obstet Invest*. 1988;25(3):165–172.
37. Gregory CD, Shah LP, Lee H, Scott IV, Golding PR. Cytotoxic reactivity of human natural killer (NK) cells during normal pregnancy: a longitudinal study. *J Clin Lab Immunol*. 1985;18(4):175–181.
38. Hanna N, Schneider M. Enhancement of tumor metastasis and suppression of natural killer cell activity by beta-estradiol treatment. *J Immunol*. 1983;130(2):974–980.
39. Hedlund M, et al. Human placenta expresses and secretes NKG2D ligands via exosomes that down- modulate the cognate receptor expression: evi- dence for immunosuppressive function. *J Immunol*. 2009;183(1):340–351.
40. Mincheva-Nilsson L, et al. Placenta-derived soluble MHC class I chain-related molecules down-regu- late NKG2D receptor on peripheral blood mono- nuclear cells during human pregnancy: a possible novel immune escape mechanism for fetal survival. *J Immunol*. 2006;176(6):3585–3592.
41. Erler JT, et al. Lysyl oxidase is essential for hypoxia-induced metastasis. *Nature*. 2006; 440(7088):1222–1226.
42. Kaplan RN, Psaila B, Lyden D. Bone marrow cells in the 'pre-metastatic niche': within bone and beyond. *Cancer Metastasis Rev*. 2006;25(4):521–529.
43. Corzo CA, et al. Mechanism regulating reactive oxy- gen species in tumor-induced myeloid-derived sup- pressor cells. *J Immunol*. 2009;182(9):5693–5701.
44. Sinha P, Okoro C, Foell D, Freeze HH, Ostrand- Rosenberg S, Srikrishna G. Proinflammatory S100 proteins regulate the accumulation of myeloid-derived suppressor cells. *J Immunol*. 2008; 181(7):4666–4675.
45. Cheng P, et al. Inhibition of dendritic cell differ- entiation and accumulation of myeloid-derived suppressor cells in cancer is regulated by S100A9 protein. *J Exp Med*. 2008;205(10):2235–2249.
46. Diaz-Montero CM, Salem ML, Nishimura MI, Gar- rett-Mayer E, Cole DJ, Montero AJ. Increased cir- culating myeloid-derived suppressor cells correlate with clinical cancer stage, metastatic tumor burden, and doxorubicin-cyclophosphamide chemothera- py. *Cancer Immunol Immunother*. 2009;58(1):49–59.
47. Bacac M, Provero P, Mayran N, Stehle JC, Fusco C, Stamenkovic I. A mouse stromal response to tumor invasion predicts prostate and breast cancer patient survival. *PLoS One*. 2006;1:e32.
48. Ferretti C, Bruni L, Dangles-Marie V, Pecking AP, Bellet D. Molecular circuits shared by placental and cancer cells, and their implications in the prolifera- tive, invasive and migratory capacities of tropho- blasts. *Hum Reprod Update*. 2007;13(2):121–141.
49. Irizarry RA, Bolstad BM, Collin F, Cope LM, Hobbs B, Speed TP. Summaries of Affymetrix GeneChip probe level data. *Nucleic Acids Res*. 2003;31(4):e15.
50. Gautier L, Cope L, Bolstad BM, Irizarry RA. affy- analysis of Affymetrix GeneChip data at the probe level. *Bioinformatics*. 2004;20(3):307–315.
51. Gentleman RC, et al. Bioconductor: open software development for computational biology and bioin- formatics. *Genome Biol*. 2004;5(10):R80.
52. Breitling R, Armengaud P, Amtmann A, Herzyk P. Rank products: a simple, yet powerful, new method to detect differentially regulated genes in repli- cated microarray experiments. *FEBS Lett*. 2004; 573(1–3):83–92.
53. Hong F, Breitling R, McEntee CW, Wittner BS, Nemhauser JL, Chory J. RankProd: a bioconduc- tor package for detecting differentially expressed genes in meta-analysis. *Bioinformatics*. 2006; 22(22):2825–2827.